

# STABILITY PERFORMANCE AND WIND TUNNEL TEST OF STEEL HYPERBOLIC COOLING TOWER CONSIDERING SKINNED EFFECT

Hui-Huan Ma<sup>1, 2, 3</sup>, Yu-Qi Jiang<sup>4, \*</sup>, Zong-Yu Li<sup>4</sup> and Zhi-Wei Yu<sup>5, \*</sup>

<sup>1</sup> School of Civil Engineering, Sun Yat-Sen University, Guangzhou, PR China

<sup>2</sup> Southern Marine Science and Engineering Guangdong Laboratory (Zhuhai)

<sup>3</sup> Guangdong Research Center for Underground Space Exploitation Technology

<sup>4</sup> Harbin Institute of Technology, 150090, China

<sup>5</sup> School of Civil Engineering, Guangzhou University, Guangzhou, P. R. China

\* (Corresponding author: E-mail: 120828422@qq.com; yuzhiwei@gzhu.edu.cn)

## ABSTRACT

With the development of industry, cooling towers play a very important role in thermal power generation, and steel cooling towers are being used more widely. The surface of cooling towers is covered with profiled panels, and the skinned effect on the mechanical performance and stability of the structure should be considered. At present, most studies on steel cooling towers have not considered the skinned effect. In steel cooling towers, the skin panels are usually connected to members by self-tapping screws., the shearing test of self-tapping screw connection is carried out considering different screw diameters and plate thicknesses to obtain the shear stiffness of the screws. Then, three FE models of steel hyperbolic cooling towers are established and compared: in Model-1, the skin panel is not considered; in Model-2, the panel and the member node are rigidly connected; in Model-3, the spring elements are established to simulate the shearing and tension stiffness of self-tapping screws connecting skin panel and members. Based on the finest Model-3, a parametric analysis is done to investigate the effect of the skinned effect on the overall structural stability. Considering different landform types and the roughness of the inner and outer surfaces, a total of 18 measurement conditions are tested in the wind tunnel to study the outer and internal wind pressure coefficients. Furthermore, based on the wind tunnel test, the wind-induced response analysis of steel hyperbolic cooling towers is performed.

## ARTICLE HISTORY

Received: 2 November 2022  
Revised: 18 April 2023  
Accepted: 10 May 2023

## KEYWORDS

Steel hyperbolic cooling tower;  
Skinned effect;  
Static stability;  
Shear stiffness;  
Tension stiffness

Copyright © 2023 by The Hong Kong Institute of Steel Construction. All rights reserved.

## 1. Introduction

The cooling tower is a large-scale building currently widely used in the power industry and machinery industry, as shown in Fig. 1. At the beginning of the 20th century, the worldwide first cooling tower was built in the Netherlands.

In the following decades, many cooling towers have been built successively in various countries, and the height of the tower has continued to increase. By the end of the 20th century, Germany and France have built very large cooling towers with a height of nearly 200m<sup>[1-3]</sup>.



(a) Reinforced concrete structure



(b) Steel structure

Fig. 1 The cooling tower structures

As the height of cooling towers becomes higher and higher, steel cooling towers has shown great potential, especially in areas with a high incidence of strong earthquakes and geological hazards, and the research on Steel Cooling Towers (SCT) has drawn more and more attention from the researchers. For the SCTs, the beam-column frame system and reticulated shell system are the two common systems. The SCTs belong to large-span spatial structures, and the stability behavior of SCTs is a prominent problem needed to be investigated in detail. A 120m SCT structure with a straight-cone-straight shape was studied<sup>[4]</sup>, and the results showed that the SCT structure with the shape has good performance and can be used for the higher structures. The nonlinear behavior of single and double-layer SCTs with different latticed shell types was compared and the optimum type was suggested for the structures with different heights<sup>[5]</sup>.<sup>6]</sup>. A linear analysis was carried out on an SCT structure with and without

stiffening rings<sup>[7]</sup>. The results showed that the stiffening rings help save material, and SCTs show good performance during earthquakes. The elasto-plastic buckling behavior under earthquake, dead and wind loads was studied<sup>[8-10]</sup>, and the study found that the forces in members and construction cost are decreased by using the buckling-restrained members. The influence of initial imperfections on the nonlinear stability of SCTs with five structural systems was studied<sup>[11,12]</sup>, and an imperfection value of H/300 was suggested as the reasonable limit for SCT design.

Another challenging issue for SCTs is the joints for connecting members in the beam-column frame system and reticulated shell system. Normally, the joints used in SCTs are welded or bolted joints, as shown in Fig. 2. The bolt joints for connecting members in steel structures have the advantage of easy installation. However, the bolted joints used in the actual SCTs are assumed to

be pin joints because of the weak bending stiffness. To solve this problem, a series of new joint types were developed [13-15], and the mechanical behavior of the new joints was investigated experimentally and numerically. The results

showed that the new joints have good stiffness and bending carrying capacity, which is suitable for SCT structures.



(a) The 181 m high cooling tower with welded joints

(b) The 124 m high cooling tower with bolted joints

Fig. 2 Steel cooling towers and joints in China

The SCTs are high-rise light self-weight structures, which belong to the wind-sensitive structures. Many studies have focused on the wind-induced response of the structures. The dynamic performance of SHCTs under wind load was studied in detail through field measurement, wind tunnel tests, and the CFD method [16-18]. The wind-reduced response and the effect of stiffening rings on the dynamic performance were discussed. The formation mechanism of non-Gaussian fluctuating wind pressures for the SCT structure was studied [19], and the forming mechanism of fluctuating wind pressure distribution was investigated in detail. The wind-induced inner and outer pressure of cylindrical-conical type SCT structure was studied [20], and a reference for wind resistance design of SCTs was obtained.

The outer surface of SCTs is covered with profiled panels. The skinned effect can strengthen the overall performance of the structure. When the structure is designed, the skin effect is only used as a reserve for stiffness and strength. Related studies by scholars have shown that the behavior of structures will be optimized under the consideration of the skinned effect, and it has been found that considering the skinned effect can help save structural costs by about 10% [21]. At present, most of the actual engineering design does not consider the strengthening effect due to the skinned effect on the structure. This design method is considered safe. However, when the skinned effect is significant, there may be skin panels may fail under normal load before the structure [22], and the study pointed out that there is still no practical design discipline for considering the skinned effect. The skinned effect of single-layer spherical aluminum alloy reticulated shell structures was studied [23], and it was obtained that the skin effect can change the buckling mode and critical load of the structure. One of the stability bearing capacities increased from 0.7 kN/m<sup>2</sup> to 2.96 kN/m<sup>2</sup>, and the effect of the aluminum plates should be considered for future structural design.

According to the summary of previous studies, it can be found that most of the research on SCT structures focuses on static analysis, elasto-plastic stability analysis, and seismic analysis, and they have not considered the skinned effect on the mechanical performance of cooling towers. Therefore, three finite element models of the SCT structure were established in this paper considering the skinned effect, conducted wind tunnel tests, and studied the wind vibration response analysis and stability analysis.

## 2. Shear performance test of self-tapping screw connection

In actual engineering projects, the skin panel and purlins fixed on the structural members are connected by self-tapping screws. In order to establish a FE model of SCT structures considering the skinned effect, the shearing test was performed to obtain the load-deformation curve of the self-tapping screws. The test specimens were made according to the recommended method in the code for the fastener test [24]. The steel sheet and the aluminum sheet were overlapped by self-tapping screws. The dimensions of the connection sheet are shown in Fig. 3. The steel grade is Q345 and the aluminum alloy grade is 6061-T6. The surface of the sheets is smooth and flat. The types of self-tapping screws are ST5.5 and ST6.3, in which 5.5 and 6.3 mean the screw diameter (mm). The test was controlled by force, and the loading speed was set to 1kN/min according to the specifications. The test mainly considered two types of parameters: plate thickness and self-tapping screw specifications. The parameter setting and the numbering rules are shown in Table 1 and Fig. 4.

Table 1 Detailed information on specimens

Numbering	$t_1$ (mm)	$t_2$ (mm)	Screw type	Screw diameter (mm)
L2-G5-5.5	2.0	5.0	ST5.5	5.5
L2-G5-6.3	2.0	5.0	ST6.3	6.3
L3-G5-5.5	3.0	5.0	ST5.5	5.5
L3-G5-6.3	3.0	5.0	ST6.3	6.3
L4-G5-5.5	4.0	5.0	ST5.5	5.5
L4-G5-6.3	4.0	5.0	ST6.3	6.3
L5-G5-5.5	5.0	5.0	ST5.5	5.5
L5-G5-6.3	5.0	5.0	ST6.3	6.3

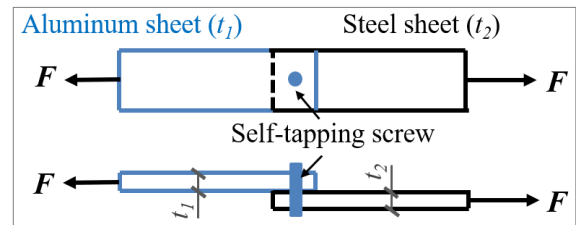


Fig. 3 Connection sheet test chart

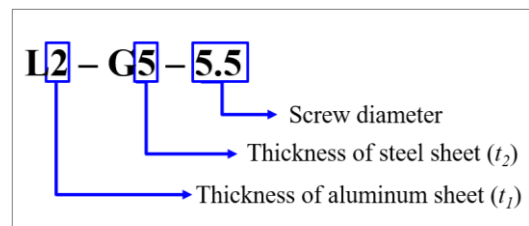


Fig. 4 Numbering rules for specimens

There are three failure modes of the specimens:

i) Failure mode 1 belongs to a kind of ductile failure modes. The screw in specimens was severely deformed, and finally was cut off. The aluminum sheet warped a little, and the screw hole on aluminum sheet was damaged, as shown in Fig. 5. This type of damage occurred in specimens L2-G5-5.5, L3-G5-5.5, and L4-G5-5.5. The load ( $L$ )-displacement ( $\Delta$ ) curves with failure mode 1 are divided into four stages: elastic stage, elasto-plastic stage, plastic stage and destruction stage, as shown in Fig. 6.

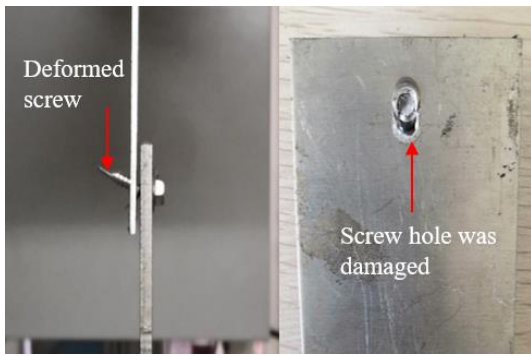


Fig. 5 Picture of failure mode 1

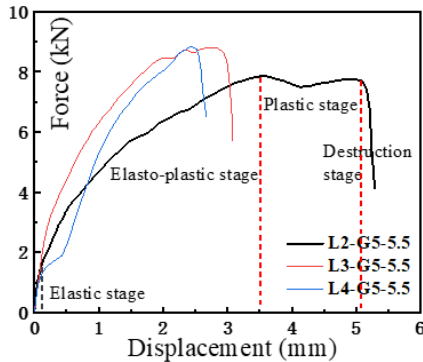


Fig. 6  $L-A$  curves of specimens with failure mode 1

ii) Failure mode 2 also belongs to a kind of ductile modes. The screw hole was cracked. There was little deformation occurred in screw, and the aluminum sheet was flat, as shown in Fig. 7. This type of damage occurred in specimen L2-G5-6.3. The  $L-A$  curve for the specimen with failure mode 2 can be divided into four stages that are similar to specimens with failure mode 1, as shown in Fig. 8.

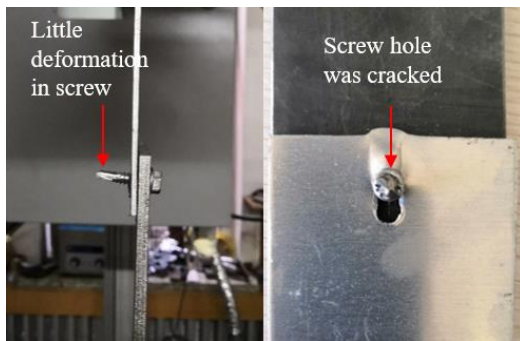


Fig. 7 Picture of failure mode 2

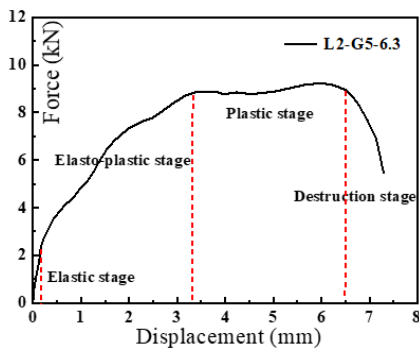


Fig. 8  $L-A$  curves of specimens with failure mode 2

iii) Failure mode 3 is a kind of brittle failure mode. The screw in the specimens was cut suddenly, and the aluminum sheet was slightly wrapped. The screw hole remained intact, as shown in Fig. 9. This type of damage occurred

in specimens L3-G5-6.3, L4-G5-6.3, L5-G5-5.5 and L5-G5-6.3. The  $L-A$  curves for the specimen with failure mode 3 are divided into three stages, as shown in Fig. 10.



Fig. 9 Picture of failure mode 3

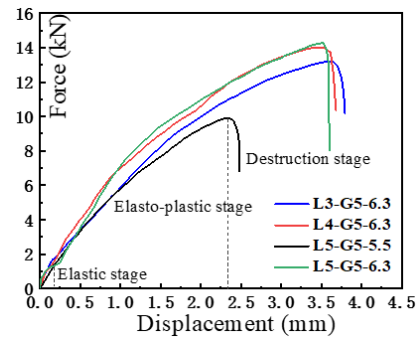


Fig. 10  $L-A$  curve specimens with failure mode 3

### 3. Static stability of SCT structures considering the skinned effect

#### 3.1. Simulation method for self-tapping screw connections

The main structure of the SCTs is mainly composed of longitudinal, circle members, diagonal members, and outer surface skin panels, as shown in Fig. 11. In this paper, three FE models of SCT structures were established to investigate the skinned effect on the stability behavior. In Model 1, the skin panel is not considered in the model; In Model 2, the aluminum skin panel is considered in the model, while the aluminum skin panel is fixed on the members through coupling the nodes of the skin plate and members. That is, the aluminum skin panels and the member nodes are rigidly connected; Model 3 is the finest model in which the spring elements are established to simulate the connection stiffness according to the actual situation between aluminum skin panels and members. In the three models, the Beam188 element is used for the longitudinal, circle and diagonal members, and the panel is simulated using the shell181 element. The panel is generally an aluminum alloy profiled plate, which is directly connected to the member by self-tapping screw at a distance of 200 mm. Since the self-tapping screw connections in structures are mainly subjected to tensile and shear forces, the self-tapping screw is simulated by establishing three combin39 spring elements in three directions of  $x$ ,  $y$ , and  $z$ , as shown in Fig. 12. The combin39 spring elements are established between the connection nodes on skin panel (1, 2, 3, etc.) and on members (1', 2', 3', etc.). The Nodes 1 and 1' are at the same coordinates in the numerical model of SCTs. Nodes 2 and 2', nodes 3 and 3', nodes 4 and 4', etc. are the same. The three combine39 elements at the connection point simulate the shear stiffness of self-tapping screws in the  $x$  and  $y$  directions and the tensile stiffness of screws in the  $z$  direction, respectively.

In ANSYS software, the  $L-A$  curves of the connections are entered by setting the real constants. Two types screws, ST5.5 and ST6.3, were used during the structure analysis. According to the results of the shear tests on self-tapping screw connections, when the thickness of aluminum and steel plate is 5 mm (specimens L5-G5-5.5 and L5-G5-6.3), the screws in specimens are cut, and the screw hole remains intact. The influence of the plates is ruled out. Therefore, the load-deformation curves of self-tapping screw specimens L5-G5-5.5 and L5-G5-6.3 can be used as the shear stiffness curves of the screws in the FE models of SCT structures, as shown in Fig. 13. The tension stiffness of the screws in the FE models of SCT structures are calculated based on the experimental study [25], as shown in Fig. 14.

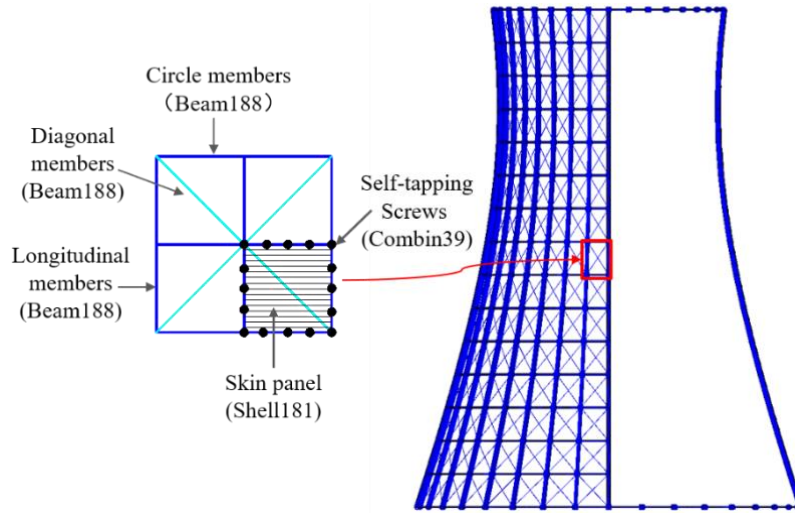


Fig. 11 Members in SCT structure

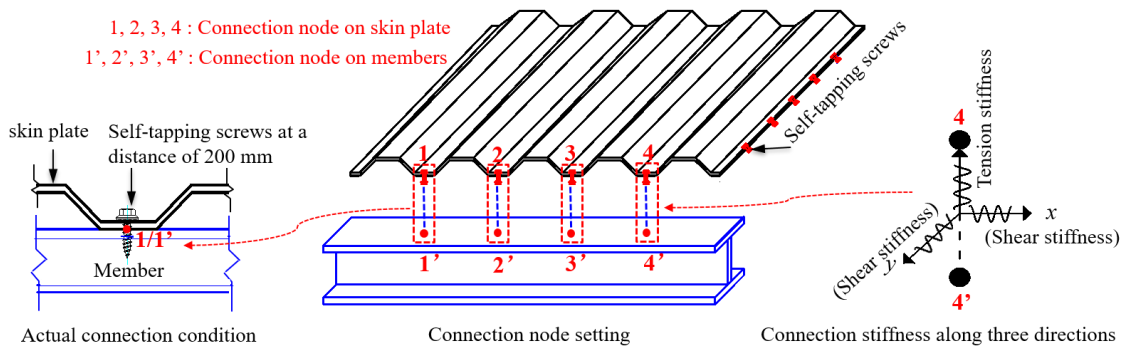


Fig. 12 Simulation method for self-tapping screw connections

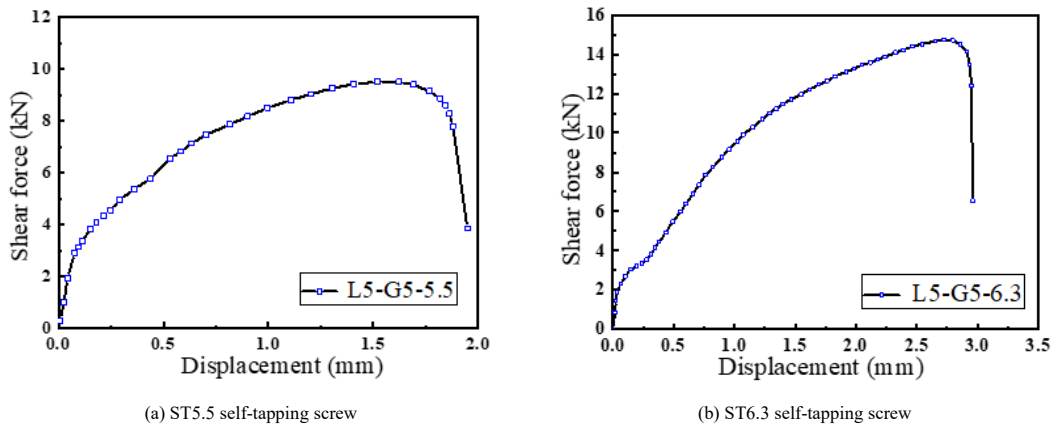


Fig. 13 Shear stiffness of self-tapping screws

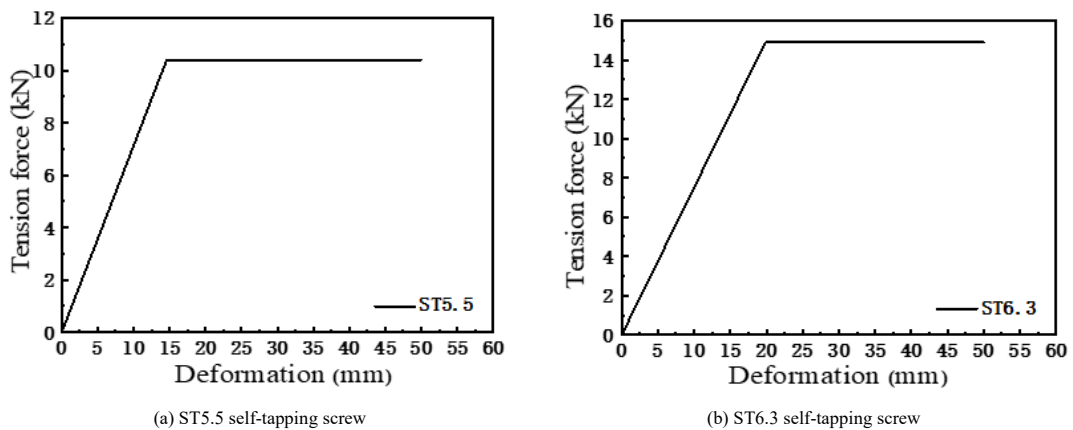


Fig. 14 Tension stiffness of self-tapping screws

### 3.2. Equivalent method of aluminum skin panel

In the real project, the surface skin panel of SCT structures is generally a profiled aluminum plate. During the parametric analysis of SCT structures, a simplified model of skin panels was established to improve computational efficiency. The shear membrane of the deck panels of a high-story steel structure was considered in the finite element analysis [26-27]. The shell element was used to simulate the cold-formed deck, which was treated as an orthogonal anisotropic deck. Based on the equivalent stiffness in three directions, an anisotropic flat plate is used instead of the isotropic profiled plate, as shown in Fig. 15.

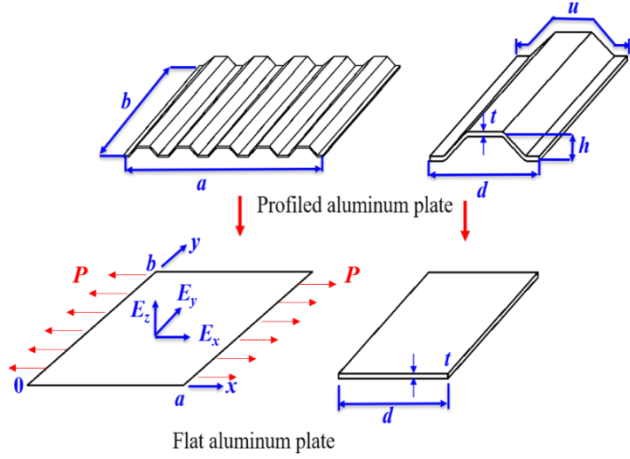


Fig. 15 Equivalent principle of the aluminum plate

The equivalent principles of the profiled plate and flat plate are: the area, length, width, and thickness of the two plates are same; the same deformation is obtained when the two plates are under same force. The material characteristics

of the profiled plate and flat plate are shown in Table 2. As shown in Fig. 15, if there is a uniformly distributed tensile force  $P$  in the direction of the plate monopod, the elongation of the profiled plate is  $\Delta_1$ , and the elongation of the equivalent plate is  $\Delta_1'$ , such that  $\Delta_1 = \Delta_1'$ , the modulus of elasticity of the profiled plate  $E'$  can be determined. The principal Poisson's ratio  $\mu_y$  of the equivalent plate is the same as the Poisson's ratio of the profiled plate.

Table 2

Material characteristics of the profiled plate and flat plate

Plate type	$E_x$ (MPa)	$E_y$ (MPa)	$\nu_{xy}$	$\nu_{yx}$	$G$	$f_{0.2}$ (Mpa)
Profiled plate	63305	63305	0.3	0.3	260	180
Flat plate	1408	75966	$6.46 \times 10^{-5}$	0.3	1300	180

### 3.3. Grid mesh method and load calculation

The hyperbolic SCT structures are usually composed of a latticed shell tower and a bottom support structure, as shown in Fig. 16. The grid size is associated with the longitudinally divided number of  $N_h$  and the circular divided number  $N_r$ .  $N_h$  equals  $H_l$  divided by  $L_h$ , which  $H_l$  is the height of the latticed shell tower, and  $L_h$  is longitudinal grid height;  $N_r$  is equal to  $360^\circ$  divided by  $\theta$ .  $\theta$  is the angle occupied by a grid around the circle. The latticed shell which is covered with profiled aluminum panels is the main study object.  $D_1$ ,  $D_2$  and  $D_3$  are the diameter of the air inlet, throat and air outlet of the SCT structure, and  $h_1$ ,  $h_2$  and  $h_3$  are the elevation of them.  $C$  is a coefficient determining the structural shape. The geometric dimension parameters of the hyperbolic SCTs are designed according to the requirements of the cooling tower design code [28], and all parameters should be set to meet the requirements of thermal calculation results. One hyperbolic line is used to generate the hyperbolic SCT structures. The equation of hyperbolic line is shown in Eq. (1).

$$\frac{X^2 + Y^2}{(D_2/2)^2} - \frac{(Z - h_2)^2}{C^2} = 1 \quad (h_1 \leq Z \leq h_3) \quad (1)$$

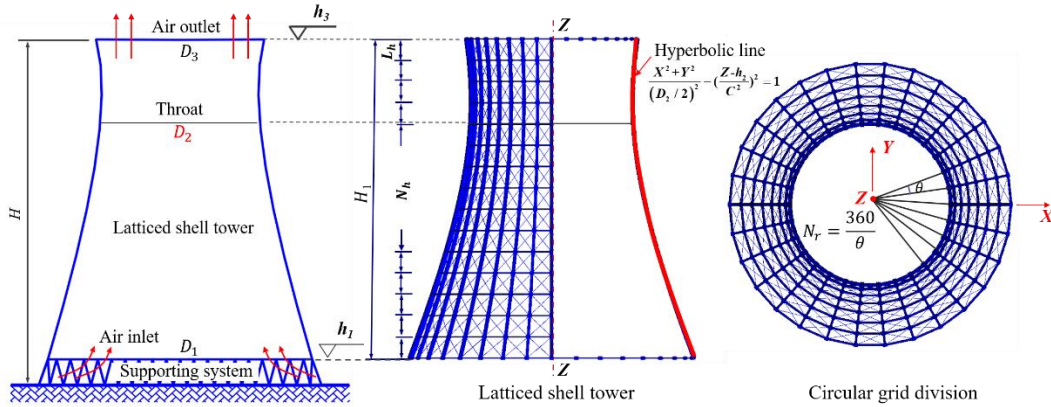


Fig. 16 Cooling tower structure diagram

During the analysis of SCT structures, the wind load and the self-weight load (steel members and aluminum skin panels) of the cooling tower considered as the main control loads were researched. The schematic diagram of the wind load was given in Fig. 17. In FE Model 1 of the SCT structure without aluminum skin panel, the wind pressure is calculated and applied to the nodes of the structure; In FE Model 2 and Model 3 of the SCT structure with aluminum skin panels, the wind load is applied to the surface of aluminum skin panel as a surface load.

According to the code [29], the standard value of the equivalent wind load on the surface is calculated by Eq. (2).  $\omega_{(z, \theta)}$  is the standard equivalent wind load (kPa) of the outer surface of the cooling tower;  $\beta = 1.9$  is the wind vibration factor.  $C_g = 1.0$  is the interference coefficient between the towers. Eq. (3) is the formula for calculating  $C_p(\theta)$ , the average wind pressure distribution coefficient.  $\mu_z$  is the height variation coefficient of wind pressure. the basic wind pressure  $\omega_0$  equals 0.55 kPa.  $\alpha_k$  and  $k$  are the coefficients for calculating  $C_p(\theta)$ , which are calculated according to the requirements of the cooling tower design code [29]. At the same time, the SCT structure has an internal wind pressure effect, and Eqs (4) and (5) are the formula for calculating the standard value of the internal wind suction. In the equations,  $\omega_i$  is the standard value of internal suction load

(kPa). The internal suction coefficient  $C_{pi}$  equals -0.5.  $q_{(H)}$  and  $\mu_H$  are the design value and the height variation coefficient of wind pressure at the top of the tower.

$$\omega_{(z, \theta)} = \beta \cdot C_g \cdot C_p(\theta) \cdot \mu_z \cdot \omega_0 \quad (2)$$

$$C_p(\theta) = \sum_{k=0}^m \alpha_k \cdot \cos k\theta \quad (3)$$

$$\omega_i = C_{pi} \cdot q_{(H)} \quad (4)$$

$$q_{(H)} = \mu_H \cdot \beta \cdot C_g \cdot \omega_0 \quad (5)$$

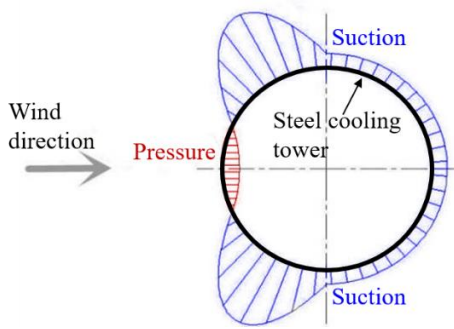
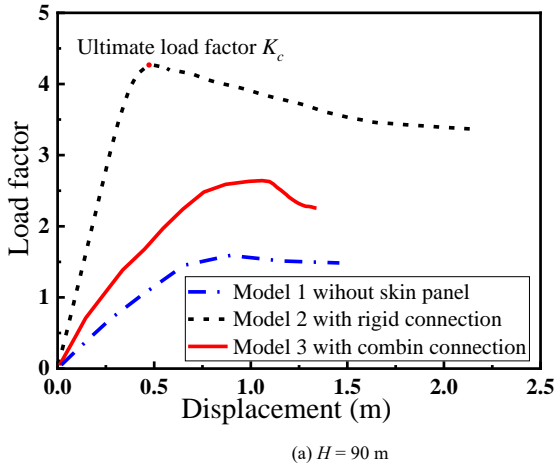
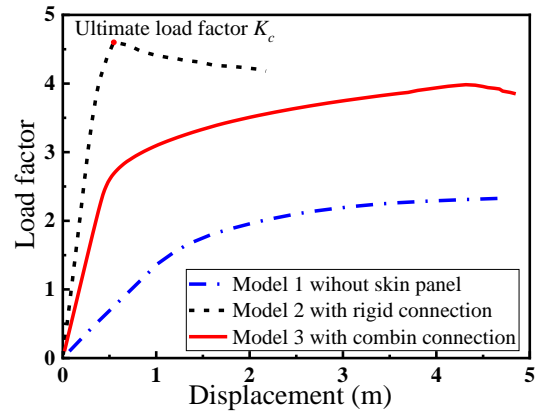


Fig. 17 Wind pressure diagram



(a)  $H = 90$  m



(b)  $H = 220$  m

Fig. 18 Load-displacement curves

Comparing the results of the three models without skin panel, the rigid joint between skin panel and members, and spring connection. The stability behavior of the SCT structure can be significantly improved by considering the skin effect. Comparing with Model-1 without skin panel, the carrying capacities obtained by Models 2 and 3 are much higher. The ultimate load factor  $\alpha_u$  of Model-3 of 90 m SCT structure with spring connections is 2.65, which is 1.67 times  $\alpha_u$  of Model-1 without skin panel.  $\alpha_u$  of Model-2 with rigid connections is 4.25, which is 2.67 times that of Model 1 without skin panel. The Model-3 of the SCT structure is the finest model, which reflect the actual situation of the real project by considering the self-tapping screw connection stiffness. The simplified Models 1 and 2 are easy to be established, but the results obtained by them cannot reflect the real mechanical behavior of SCT structures.

3.5. Parametric stability analysis of SCT structures considering the skinned effect

In order to comprehensively analyze the stability performance of the SCT structures considering skinned effect, four heights of 90 m, 130 m, 180 m, and 220 m are selected, and different grid sizes are designed. The specific size settings are shown in Table 3 below. For the SCT structures with different heights, six grid sizes ( $G_1 \sim G_6$ ) from small to large are considered. For the SCT structure with each height and grid size, the skinned and unskinned structural models are analyzed and compared. The finest Model-3 of the SCT structure is used to carry out the parametric analysis. The dual nonlinear stability analysis was carried out on 48 models with different heights and grid sizes.

3.5.1. Typical example analysis

Based on the finest Model-3 of SCT structure with 90 m height and  $G_2$  grid size, the stiffness state of the screwed connections and stress state in the panels were studied. Three points are plotted on the  $L-A$  curves (Fig. 19) of SCT with 90 m height and  $G_2$  grid size. Point 1 is the upper limit of the linear stage of the structure. Point 2 corresponds to the critical load factor. Point 3 is the end point of the calculation.

Fig. 20 shows the stress distribution of the panels of SCT corresponding to

3.4. Comparison of the three FE models

Two-height single-layer rectangular SCTs are selected for analysis considering the geometric and material nonlinearity to show the effect of the simulation method of self-tapping screw connection and the stressed-skin on the stability behavior of SCT structures. Three FE models of 90 m and 220 m SCT structures are established respectively. In Model-1, the skin panel is not considered. In Model-2, the panel and the member node are rigidly connected. In Model-3, the spring elements are established to simulate the connection stiffness according to the actual situation between skin panel and members. The full process  $L-A$  curves are shown in Fig. 18.

the three key points. It can be found that a large number of panels at bottom and a small number of panels in the middle of SCT yield at Point 1. At Point 2, the yield area in the middle expands to the suction area of the SCT. The local buckling that happens at Point 3 leads to the failure of the structure. As shown in Fig. 21, lots of self-tapping screw connections enter elastic stage due to shear force or tension force. The self-tapping screw connections enter elastic stage due to shear force mostly in the middle and bottom pressure area and side suction area of the structure. The self-tapping screw connections enter the plastic stage due to shear force is mostly in the middle and bottom pressure area.

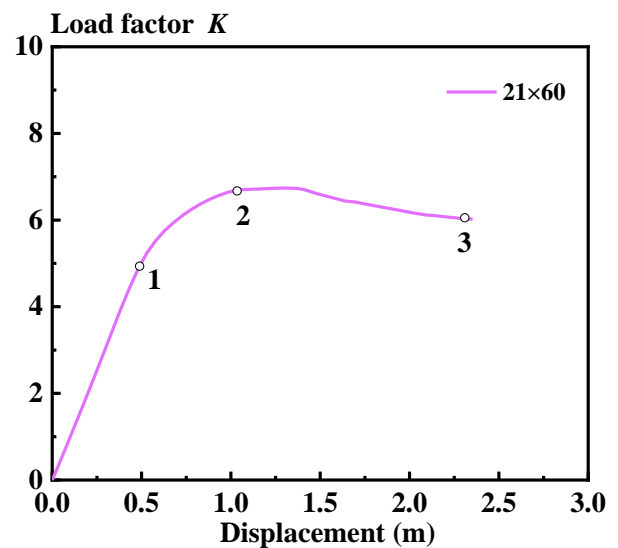


Fig. 19 Load-displacement curves of SCTs with 90 m height and  $G_2$  grid size

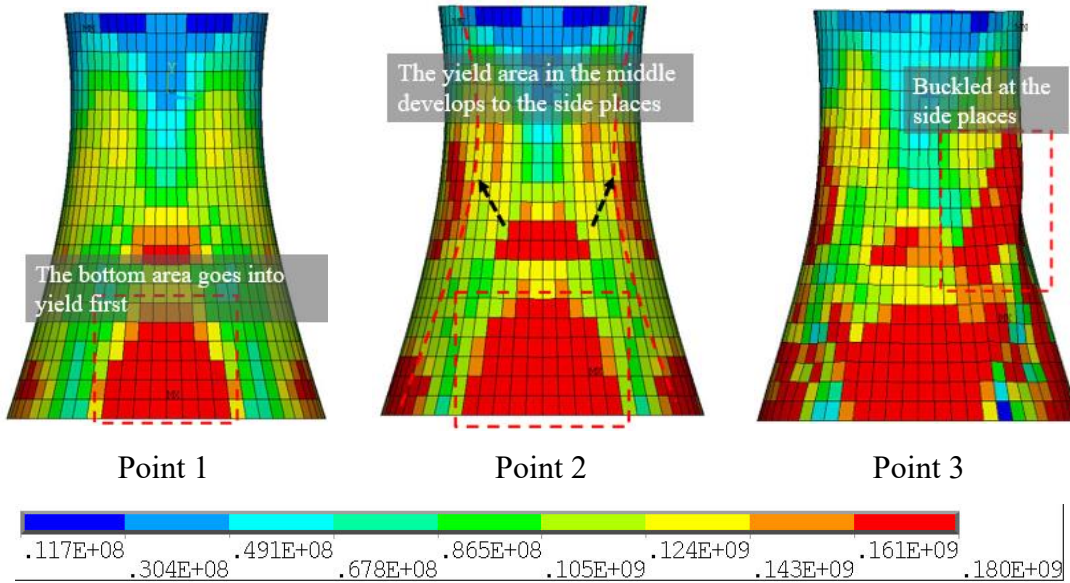


Fig. 20 Stress distribution of the panels of SCTs with 90 m height and  $G_2$  grid size

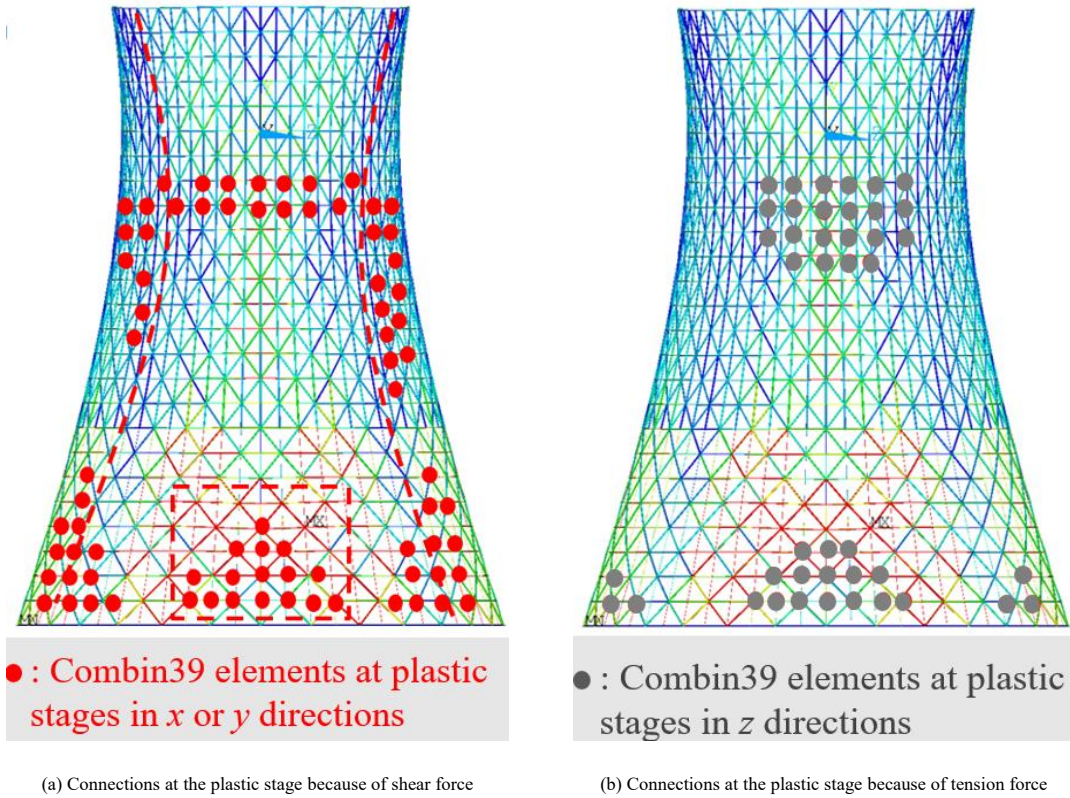


Fig. 21 The self-tapping screw connections at plastic stage

3.5.2. Results of parametric stability analysis

The whole load-displacement curves are shown in Fig. 22. For each height grid size, two models with and without skin were calculated. The solid lines in the figures are obtained by Model 3 with skin panels, and the dashed line is obtained by Model 1 without skin panels. The ultimate bearing capacity of the

skinned structure is represented by  $K_{crs}$ , and the ultimate bearing capacity of the unskinned structure is represented by  $K_{cr}'$ , as shown in Fig. 23 and Table 4. The change law of  $K_{cr}/K_{cr}'$  which can reflect the skinned effect on the bearing capacity, as shown in Fig. 24.

Table 3  
Parameter scheme for height and grid size

Height $H(m)$	Grid size $N_n \times N_r$	Air inlet size (m <sup>2</sup> )	Throat size (m <sup>2</sup> )	Air outlet size (m <sup>2</sup> )
90	$G_1$ 25×72	3.37×2.89	3.37×1.69	3.37×1.81
	$G_2$ 21×60	4.01×3.47	4.01×2.03	4.01×2.17
	$G_3$ 17×40	4.95×5.21	4.95×3.05	4.95×3.26
	$G_4$ 15×36	5.61×5.78	5.61×3.39	5.61×3.62

130	$G_5$	13×30	6.48×6.94	6.48×4.06	6.48×4.34
	$G_6$	11×24	7.65×8.68	7.65×5.08	7.65×5.43
	$G_1$	35×72	2.9×2.96	2.9×2.10	2.9×2.20
	$G_2$	31×60	3.27×3.56	3.27×2.52	3.27×2.64
	$G_3$	27×50	3.76×4.27	3.76×3.01	3.76×3.17
	$G_4$	25×40	4.06×5.34	4.06×3.79	4.06×3.96
180	$G_5$	21×36	4.83×5.93	4.83×4.21	4.83×4.40
	$G_6$	17×24	5.97×8.89	5.97×6.31	5.97×6.60
	$G_1$	55×72	3.00×4.95	3.00×2.97	3.00×3.05
	$G_2$	45×60	3.67×5.94	3.67×3.56	3.67×3.66
	$G_3$	35×50	4.71×7.13	4.71×4.27	4.71×4.39
	$G_4$	33×48	5.00×7.43	5.00×4.45	5.00×4.57
220	$G_5$	25×40	6.60×8.91	6.60×5.34	6.60×5.49
	$G_6$	21×36	7.86×9.90	7.86×5.94	7.86×6.10
	$G_1$	45×80	4.21×6.91	4.21×5.45	4.21×5.60
	$G_2$	35×72	5.41×7.68	5.41×6.06	5.41×6.23
	$G_3$	33×60	5.74×9.22	5.74×7.27	5.74×7.47
	$G_4$	29×50	6.53×11.06	6.53×8.73	6.53×8.97
	$G_5$	25×48	7.58×11.52	7.58×9.09	7.58×9.34
	$G_6$	21×40	9.02×13.83	9.02×10.91	9.02×11.21

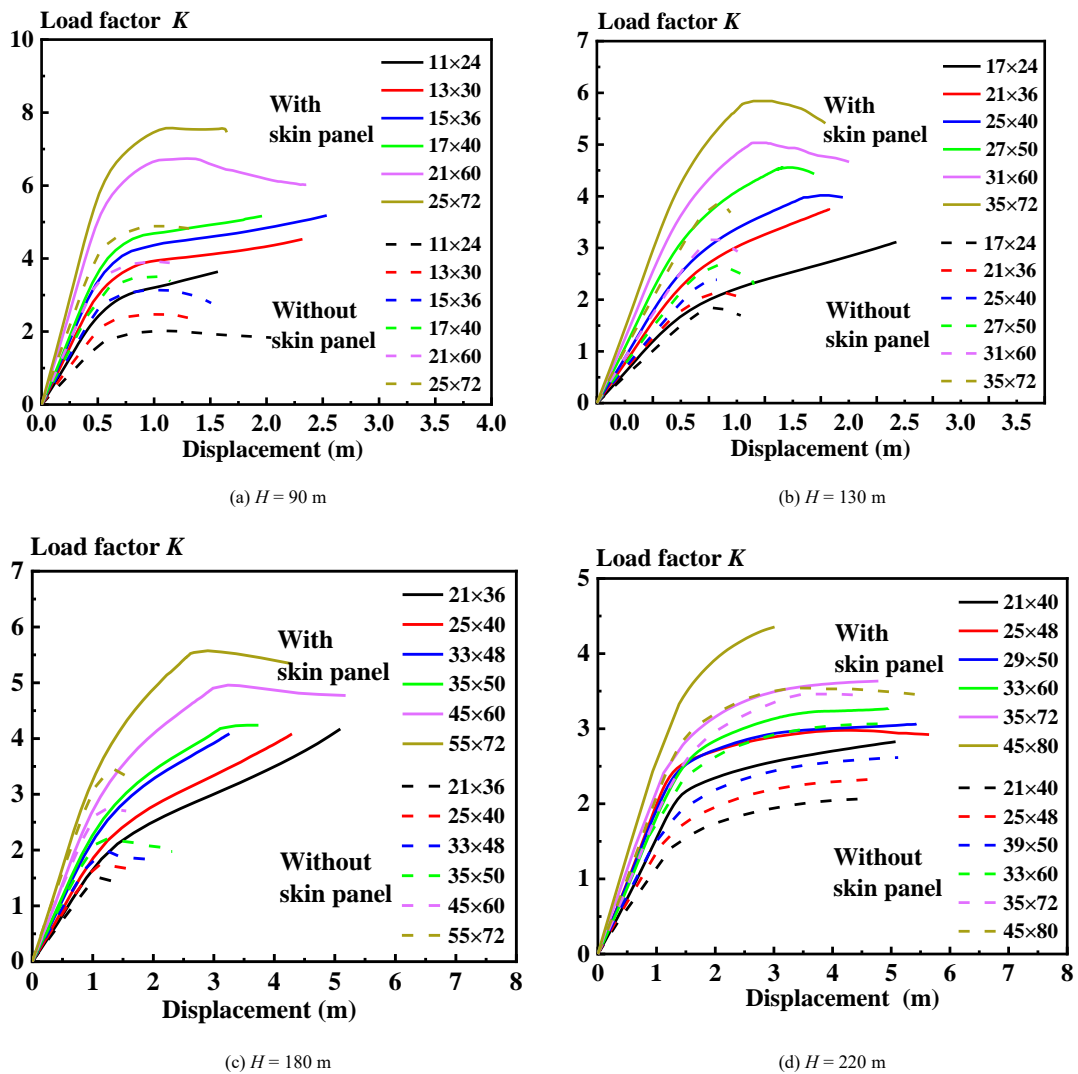


Fig. 22 Load-displacement curves of SCTs with different heights and grid sizes



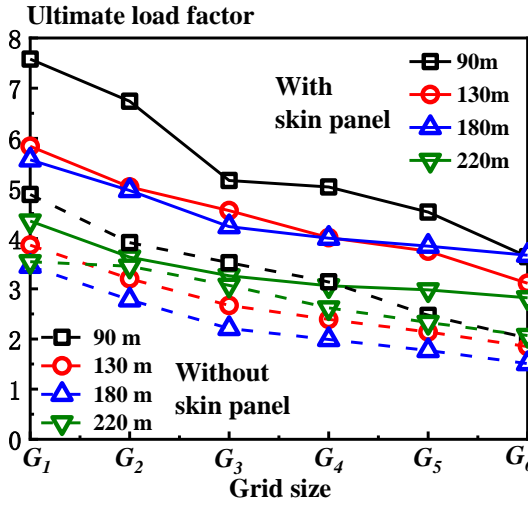


Fig. 23 Comparison of ultimate carrying capacity at different heights

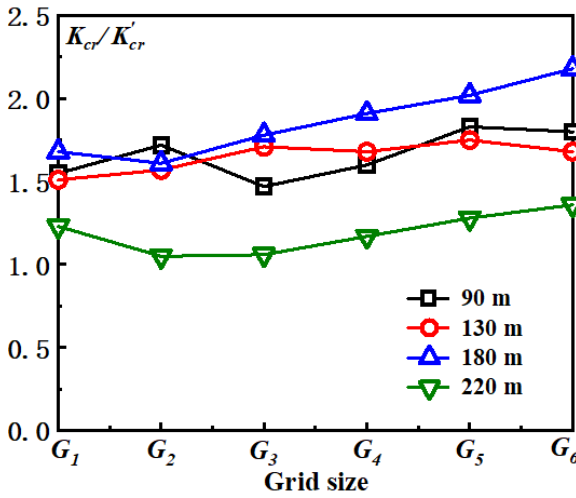


Fig. 24 Chang law of  $K_{cr}/K_{cr}'$

It can be concluded that at the same height, as the grid size increases,  $K_{cr}$  and  $K_{cr}'$  decrease, and  $K_{cr}/K_{cr}'$  represents the skinned effect on the ultimate bearing capacity. The grid size becomes larger, and  $K_{cr}/K_{cr}'$  gradually increases, indicating that as the grid becomes larger, the skinned effect on the bearing capacity gradually increases.

Table 4 Ultimate bearing capacity of SCTs with different heights and grid sizes

Height $H$ (m)	Grid size	$N_R \times N_F$	$K_{cr}$	$K_{cr}'$	$K_{cr}/K_{cr}'$
90	$G_1$	25×72	7.58	4.88	1.55
	$G_2$	21×60	6.74	3.92	1.72
	$G_3$	17×40	5.16	3.52	1.47
	$G_4$	15×36	5.03	3.14	1.60
	$G_5$	13×30	4.53	2.47	1.83
	$G_6$	11×24	3.64	2.02	1.80
130	$G_1$	35×72	5.84	3.87	1.51
	$G_2$	31×60	5.03	3.20	1.57
	$G_3$	27×50	4.56	2.67	1.71
	$G_4$	25×40	4.02	2.39	1.68
	$G_5$	21×36	3.75	2.14	1.75
	$G_6$	17×24	3.11	1.85	1.68
180	$G_1$	55×72	5.57	3.45	1.61
	$G_2$	45×60	4.96	2.78	1.78
	$G_3$	35×50	4.24	2.21	1.91

$G_4$	33×48	4.01	1.99	2.02	
$G_5$	25×40	3.85	1.77	2.18	
$G_6$	21×36	3.67	1.51	2.43	
$G_1$	45×80	4.35	3.54	1.23	
$G_2$	35×72	3.63	3.45	1.05	
$G_3$	33×60	3.26	3.07	1.06	
220	$G_4$	29×50	3.06	2.62	1.17
	$G_5$	25×48	2.98	2.33	1.28
	$G_6$	21×40	2.82	2.07	1.36

The following table 5 is the comparison of the maximum displacement of cooling towers with different grid sizes at the height of 90 m. It indicated that the maximum displacement of the structure decreased with decreasing grid size. However, the stiffness increased with decreasing grid size. Comparing the maximum displacement of skinned and non-skinned SCTs with the same grid, the maximum displacement of the skin structure is smaller than that of the non-skinned structure, because the overall skin panel on SCTs increases the stiffness and reduces the displacement. Compared with the reduction ratios of the maximum displacement, it can be seen that when the grid size is smaller, the reduction ratio of the maximum displacement is larger. As the mesh size becomes larger, the reduction ratio gradually decreases, indicating that the denser the mesh, the denser the skin panel, and the stronger the skinned effect, the greater the increase in structural stiffness.

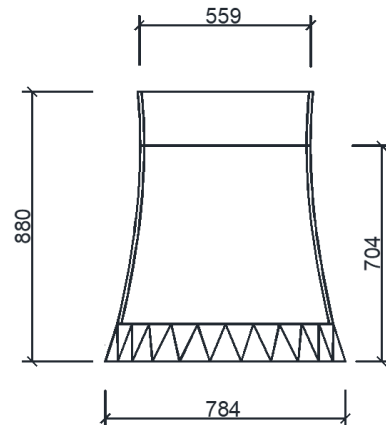
Table 5 Comparison of maximum displacements of 90 m SCTs (m)

Models	Grid size					
	$G_1$	$G_2$	$G_3$	$G_4$	$G_5$	$G_6$
Skinned structure	1.65	2.01	3.34	4.61	4.74	4.97
Non-skinned structure	2.13	2.49	3.78	5.21	5.45	5.79
Reduction ratio	29.1%	23.1%	13.2%	13.1%	15%	16.5%

#### 4. Wind tunnel test and wind-induced response analysis of hyperbolic SCT structures

##### 4.1. Wind tunnel test

At present, the wind tunnel test is currently the most commonly used method for obtaining wind loads in the field of wind engineering. It is relatively easy to implement and measure and can provide a design basis before building construction. The wind tunnel test was conducted in the wind tunnel and wave trough joint laboratory of the HIT. The size of the test model was designed according to the actual parameters of the 220m SCT structure under design in Zhaozhuang, Shanxi province of China (see Fig. 25(a)). The scale ratio is 1: 250 according to the requirements of the wind tunnel laboratory. The wind tunnel test model is made of an acrylic sheet (Plexiglas sheet) and a plastic sheet, as shown in Fig. 25(b). Table 6 lists the specific dimensions of the cooling tower model and prototype.



(a) The size of the test model



(b) Picture of the test model

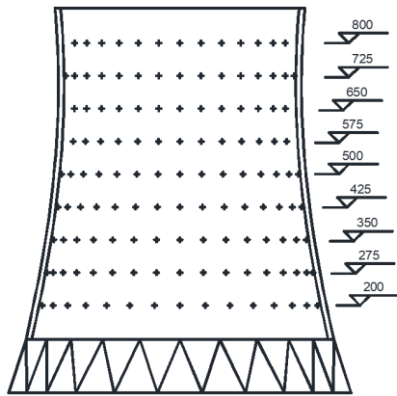
Fig. 25 The test model

**Table 6**  
Cooling tower prototype and model dimensions

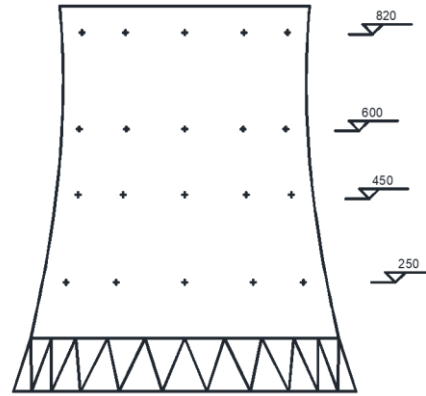
SCT	$H$	$h_1$ (m)	$D_1$ (m)	$h_2$ (m)	$D_2$ (m)	$h_3$ (m)	$D_3$ (m)
Prototype	220	30.5	179.3	176	138.9	220	142.7
Test model	0.88	0.122	0.717	0.704	0.556	0.88	0.571

The arrangement of measuring points considers both external pressure and internal pressure. The external and internal pressure measuring points were evenly arranged along circumferential direction and the meridional direction of the test model. The total number of measurement points arranged on the test model was 372, as shown in Fig. 26.

In this paper, the Reynolds number effect was simulated by changing the surface roughness. There are mainly two simulation methods, one is sticking tape on the surface, and the other is sticking sandpaper on the surface. 36 pieces of tape or sandpapers at a distance of about 6mm were pasted on the outer surface of the cooling tower model, as shown in Fig. 27. At the same time, considering that the inner steel members of the SCT structure may have some influence on the internal pressure, a sponge bar was fixed to the internal surface of the test model to simulate the internal members. 6×16 strips with 1cm×1cm specifications were arranged in the ring direction and the meridian direction, as shown in Fig. 28.



(a) External pressure measuring point



(b) Internal pressure measuring point

Fig. 26 The measuring point layout on the test model

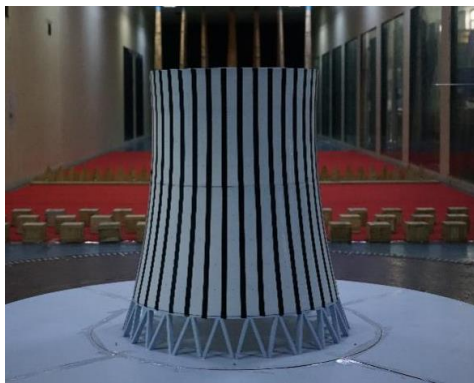
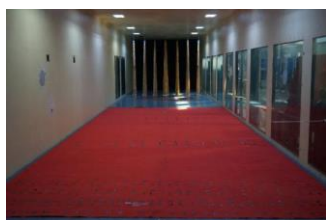


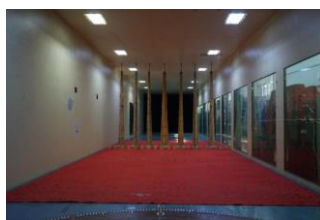
Fig. 27 Reynolds number effect simulation



Fig. 28 Internal member simulation



(a) A type



(b) B type



(c) C type

Fig. 29 Three planform types

In this test, three types of landforms, A type, B type, and C type, were considered. The passive simulation method was used for wind field simulation by placing spikes, baffles, rough elements, and carpets. The pictures of the three

landform types are shown in Fig. 29. According to the landform type, the roughness of the inner and outer surfaces, and a total of 18 measurement conditions have been set, as shown in Table 7.

**Table 7**

Measurement conditions

Conditions	Landform type	Inner members	Outer roughness simulation
1			Smooth
2		Yes	Tapes
3	A		sandpapers
4			Smooth
5		No	Tapes
6			sandpapers
7			Smooth
8		Yes	Tapes
9	B		sandpapers
10			Smooth
11		No	Tapes
12			sandpapers
13			Smooth
14		Yes	Tapes
15	C		sandpapers
16			Smooth
17		No	Tapes
18			sandpapers

The wind pressure values at different heights under different working conditions were obtained. The average wind pressure coefficient of the test models with smooth surface, tapes on the surface, and sandpapers on the surface were compared with the standard curve in the cooling tower design code [29], as shown in Fig. 30. In order to compare the changes of wind pressure on the cooling tower surface under different wind speeds, three wind speed were carried out in the test. The model with adhesive tape on surface was taken as an example. The average wind pressure coefficients of the test model under different wind speeds were shown in Fig. 31. It can be obtained that: changing the surface roughness has a greater influence on the extreme value of the wind suction; the width of the wind suction area at the leeward side of the structure; the wind pressure coefficients obtained by the model setting surface tapes is

closer to that in the cooling tower design code [29], and changing wind speed has little effect on the wind pressure coefficient.

Fig. 32 is a comparison diagram of the internal pressure at different heights under two working conditions: smooth inner surface and sponge surface. It can be obtained that the internal pressure coefficient obtained by the test is slightly larger than that in the cooling tower design code [29], and the internal pressure gradually increases with decreasing height. The internal pressure value at the bottom measurement point is more unstable, and the suction point appears on the leeward surface. By comparing the test models with smooth internal surface and internal surface sticking sponge strips, the internal sponge strip has a certain effect on the wind pressure value of the internal wind field, and it is not much different from the values in the cooling tower design code [29].

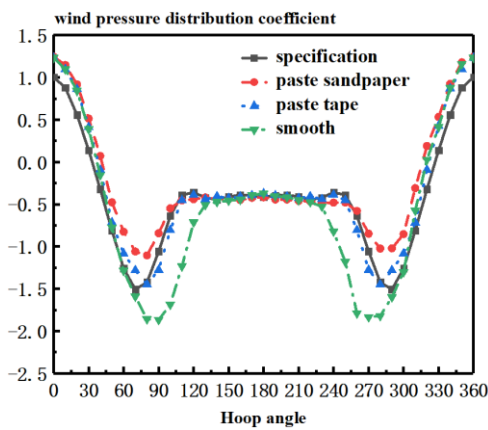


Fig. 30 Comparison of wind pressure coefficient at throat height

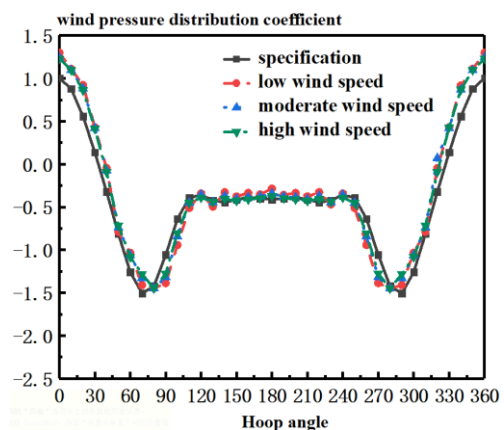
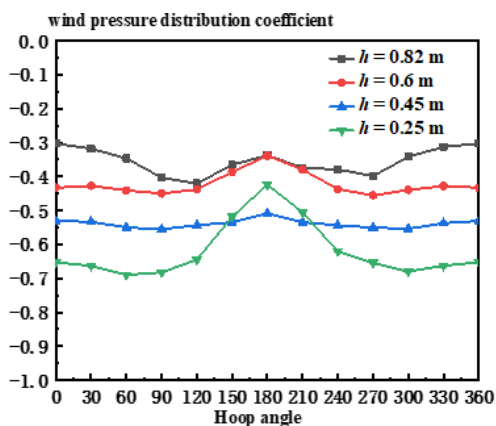
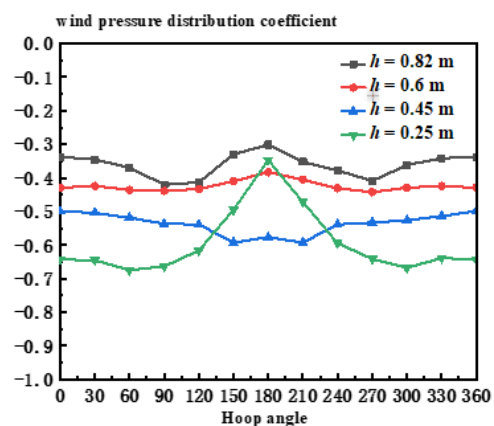


Fig. 31 Comparison of average wind pressure coefficients at different wind speeds



(a) Smooth inner surface



(b) Inner surface with spongy strips

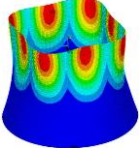
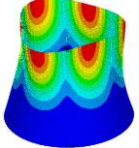
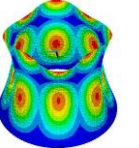
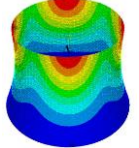
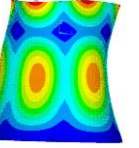

Fig. 32 Comparison of internal pressure at different heights

4.2. Wind-induced response analysis of SCT structures

First, the dynamic characteristics of the structure, including the mode shape and frequency, were analyzed. The SCT structure with  $H = 220$  m, grid size  $45 \times 80$ , and panel thickness of 2 mm was taken as an example. The first 40 modes

and frequencies of the structure were extracted according to the Model 3, established previously. The following Table 8 gives the main several mode shapes, frequencies, and mode characteristics of the SCT structure considering the skinned effect.

**Table 8**  
Mode shapes and frequencies of SCT structures

Order	1, 2	3, 4	7, 8	11, 12	17, 18	33, 34
Frequency	0.67	0.70	0.92	0.98	1.17	1.66
Shape characteristics	4 toroidal harmonics	3 toroidal harmonics	4 toroidal harmonics; 3 vertical harmonics	Hoop compression	3 toroidal harmonics; 2 vertical harmonics tilt	Vertical compression
Mode shape						

The hyperbolic tower is symmetric, and the mode shapes of the structure appear in pairs. From the frequency results, the first few modes of the structure mainly show a combination of several ring harmonics and vertical harmonics; the first few modes are symmetrical deformation and lower frequency; more complex modes appear after the 15th order, and there is a lateral tilt under the combination of hoop harmonics and vertical harmonics; vertical compression modes appear only after the 30th order. It shows that the torsional stiffness and lateral stiffness of the hyperbolic cooling tower are small, while the vertical stiffness is large.

The wind load time-history data obtained from the wind tunnel test is interpolated and encrypted to investigate the wind-induced response of hyperbolic SCT structures. The wind load data is interpolated by the POD method based on the wind tunnel test points. The wind pressure data for a total

of 3600 points are obtained, which is the same as the node number in the SCT structure model. The wind load data at each point position is imported into the model to carry out the transient dynamic analysis. The loading time interval is converted to 0.1s according to the sampling frequency of the wind tunnel test. The displacement time history of each node of the structure can be obtained. The displacement distribution of the nodes along the circular direction at the top of the tower and the nodes at  $0^\circ$  meridians along the height were plotted, as shown in Fig. 33. The above figures show that the displacement response of the tower top is the largest and basically symmetrical along the horizontal axis. The displacement in the leeward area is small. Along the meridian direction, the displacement increases moderately with the increasing height, reaches a peak at the left and right positions of the throat, and then decreases a little.

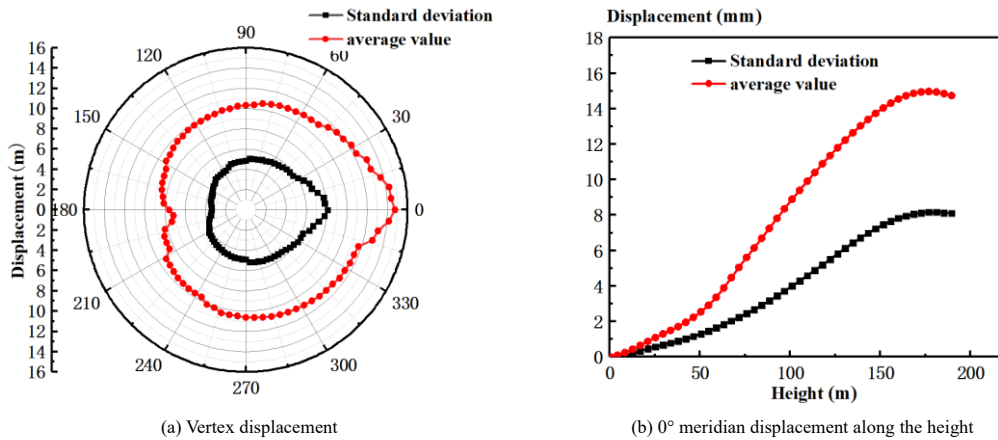


**Fig. 33** Distribution of displacement response

The wind vibration factor is usually represented by the ratio of the structure's maximum response to its average response, which can reflect the amplification effect on the turbulent wind. This paper mainly solves the wind vibration factors, and defines the wind vibration factors of a point as the ratio of the maximal displacement response to the average displacement response of the point. After extracting the displacement time history of, the average and standard deviation of the displacement can be obtained. Therefore, the displacement wind vibration factor  $G_x$  can be obtained by the following formula:

$$G_x = \frac{X_{max}}{X_{ave}} = 1 + g \frac{\sigma_x}{X_{ave}} \quad (6)$$

among them,  $G_x$  is the displacement wind vibration factor at a certain position of the structure and  $X_{max}$ ,  $X_{ave}$ ,  $\sigma_x$  are maximum, average, and standard deviation vibration displacement response of the wind vibration displacement of the structural at position;  $g$  is the crest factor of the structural displacement response, which is generally taken as 3-4 according to related theories, and 3 is taken in this paper.

The SCT structure is more complex and has more nodes. This paper only

gives the displacement wind vibration factors at several angles, as shown in Table 9 below. The meridional and annular directions are plotted to more clearly reflect the distribution of the wind vibration factors. The change law of the wind vibration factors along the vertical and circumferential direction of the SCT structure with a height of 220 m is shown in Fig. 34 which shows that the wind vibration factors are symmetric along the horizontal direction.

**Table 9**  
Value of the wind vibration factor ( $H = 220$  m)

Parameter	Height $h$ (m)	Angle				
		$0^\circ$	$45^\circ$	$90^\circ$	$135^\circ$	$180^\circ$
Wind vibration factor $G$	219.45	2.04	2.36	2.48	2.68	3.06
	173.14	1.89	2.28	2.46	2.78	3.07
	126.83	2.12	2.36	2.49	2.61	2.91
	84.73	2.25	2.55	2.66	2.83	2.73
	46.84	2.51	2.72	2.82	2.53	2.47

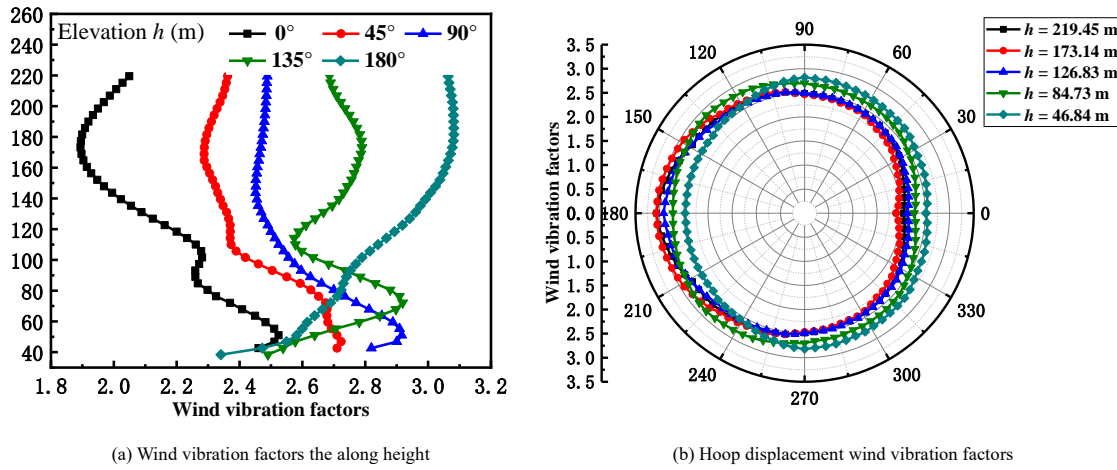


Fig. 34 Wind vibration factors along the vertical and circumferential direction

5. Conclusions

A series of shearing tests was conducted on the self-tapping screwed connections to investigate the connection performance. The *L-A* curves of specimens with different plate thicknesses and screw diameters were obtained and analyzed. Two ductile failure modes and one brittle failure mode happened during the test.

Based on experimental shear stiffness curves of self-tapping screw connection, three FE models of steel hyperbolic cooling towers with and without skin panels were established. By comparing the results of the three models, it is found that the stability behavior of SCT structure obtained by three modes is much different. The ultimate load factor  $\alpha_u$  of Model-3 of 90 m SCT structure with spring connections is 2.65, which is about 2 times  $\alpha_u$  of Model-1 without skin panels.  $\alpha_u$  of Model-2 with rigid connections is 1.60 times that of Model-3 with a spring connection. Based on the parametric analysis of SCT structures, the stability behavior of SCT structure can be significantly improved by considering the skin effect, and as the grid size increases, the skinned effect on the ultimate bearing capacity increase gradually.

Based on the wind tunnel test, changing the surface roughness has a greater influence on the extreme value of the wind suction area and the width of the leeward suction area. The wind pressure coefficients obtained by the model setting surface tapes are closer to that in the cooling tower design code. Changing wind speed has little effect on the wind pressure coefficient. By comparing the test models with smooth internal surface and internal surface sticking sponge strips, the internal sponge strip has a certain effect on the wind pressure value of the internal wind field. The wind vibration factors are symmetric along the horizontal direction.

Acknowledgement

This research was supported by the National Key R&D Program of China (grant no. 2018YFC0705500, 2018YFC0705504)

References

[1] D. Busch, R. Harte, W. B. Krätzig, U. Montag. New natural draft cooling tower of 200 m of height. *Eng. Struct.* 2002; 24(12): 1509-1521.  
 [2] D. Busch, R. Harte, W. B. Krätzig, U. Montag. World's Tallest Natural Draft Cooling Tower, near Cologne, Germany. *Struct Eng. Int.* 2001; 11(2):107-109.  
 [3] R. Harte, W.B. Krätzig, Large-scale cooling towers as part of an efficient and cleaner energy generating technology, *Thin-Walled Struct.* 40 (7) (2002) 651–664, [https://doi.org/10.1016/S0263-8231\(02\)00018-6](https://doi.org/10.1016/S0263-8231(02)00018-6).  
 [4] L. Kollar, Large reticulated steel cooling towers, *Eng. Struct.* 1985; 7 (4): 263–267  
 [5] H. Ma, S. Li, F. Fan, Static performance analysis of single-layer steel cooling tower, *Structure* 2019; 19: 322–332, [https://doi.org/10.1016/S0141-0296\(98\)00138-2](https://doi.org/10.1016/S0141-0296(98)00138-2)  
 [6] H.H. Ma, Z.Y. Li, S.Z. Li, B.B. San, F. Fan, Stability analysis and performance comparison of large-scale hyperbolic steel cooling towers with different latticed shell systems, *J Constr*

*Steel Res.* 2019; 160: 559-578. <https://doi.org/10.1016/j.jcsr.2019.05.042>  
 [7] M. Izadi, K. Bargi. Natural draft steel hyperbolic cooling towers: Optimization and performance evaluation. *Struct. Design Tall Spec. Build.* 2014; 23:713-720.  
 [8] S. Kato, S. Nakazawa, S. Shimaoka, et al., Effectiveness of buckling restrained members for diagonal columns to reduce the seismic response of cooling towers, *Natural Draught Cooling Towers*, 2004.  
 [9] S. Kato, S. Shimaoka, H. Okada, et al., A study on buckling and earthquake-resistant capacities for steel cooling towers, *J. Struct. Constr. Eng.* (2005) 85–92.  
 [10] F. Pourshargh, F. P. Legeron, S. Langlois and K. Saoud. A simple method for a reliable modelling of the nonlinear behaviour of bolted connections in steel lattice towers. *Advanced Steel Construction* 2022, 18(1): 479-487.  
 [11] J. Wu, J.Y. Zhu, Y. Dong, Q.L. Zhang. Nonlinear stability analysis of steel cooling towers considering imperfection sensitivity, *Thin-walled Struct* 2020; 146: 106448. <https://doi.org/10.1016/j.tws.2019.106448>  
 [12] F. Wang, K. Zhou and S. Ke. Research on dynamic load carrying capacity of assembled internal stiffening wind turbine tower based on multi-scale modeling. *Advanced Steel Construction* 2023, 19(1): 86-90.  
 [13] H.H. Ma, Y. Zhao, F. Fan, Z.W. Yu, X.D. Zhi, Experimental and numerical study of new connection systems for a large-span hyperbolic steel cooling tower, *Eng. Struct.* 2019; 195: 452-468.  
 [14] H. Ma, C. Zhao, Y. Jiang, G. Zhou and Y. Wang, Rotational resistance test of a new aluminum alloy penetrating (AAP) joint system. *Advanced Steel Construction* 2023, 19(2): 121-129.  
 [15] Y. Jiang, H. Ma, G. Zhou and F. Fan. Parametric and comparison study of a new and traditional aluminum alloy joint systems. *Advanced Steel Construction* 2021, 17(1): 50-58.  
 [16] S.T. Ke, L.Y. Du, Y.J. Ge, L. Zhao. A study on the average wind load characteristics and wind-induced responses of a super-large straight-cone steel cooling tower. *Wind Struct* 2017; 25(5): 433-457  
 [17] J.F. Zhang, Y.J. Ge, S.T. Ke. Effects of stiffening rings on the dynamic properties of hyperboloidal cooling towers. *Struct Eng Mech* 2014; 49(5): 619-629.  
 [18] Y. Wang, S. Wang, X. Zhou, etc. Buckling behavior of the steel plate in steel – concrete – steel sandwich composite tower for wind turbine. *Advanced Steel Construction* 2022, 18(3): 699-706.  
 [19] Ke S, Wang H, GeY. Non-Gaussian characteristics and extreme distribution of fluctuating wind pressures on large cylindrical-conical steel cooling towers. *Struct Design Tall Spec Build.* 2017;26: e1403. <https://doi.org/10.1002/tal.1403>  
 [20] Ke S, Du L, Ge Y. Wind-induced internal pressure effect within a novel super-large cylindrical-conical steel cooling tower. *Struct Design Tall Spec Build.* 2018;27: e1510. <https://doi.org/10.1002/tal.1510>  
 [21] J.M. Davies, E.R. Bryan, *Manual of Stressed Skin Diaphragm Design*. New York: Granada Publishing, 1982.  
 [22] Y.L. Shi, X.L. Wang, *Development and Research of Stressed Skin Diaphragms*. *Spatial Structures* 2004; 19(4): 10-13. (in chinese)  
 [23] H.B. Liu, Z.H. Chen, S. Xu, et al. Structural Behavior of Aluminum Reticulated Shell Structures Considering Semi-Rigid and Skin Effect. *Struct Eng Mech.* 2015; 54(1): 121 – 133.  
 [24] *Fastener test methods-Lap joint shear*. GJB715.19-90.  
 [25] Y.Q. Li, Y.Q. Shuai, Z.Y. Shen, Y.F. Qin, Y.Q. Chen. Experimental study on tension behavior of self-drilling screw connections for cold-formed thin-walled steel structures. *Journal of Building Structures* 2015; 36(12): 143-152.  
 [26] H.Y. Wan, M. Wang, D. Zeng. Finite element analysis of high-story steel structure in case of shear-resistant membrane, *Journal of Hefei University of Technology* 2001; 24(2): 184-188 (in Chinese).  
 [27] A.H. Nilson, A.R. Ammar. *Finite Element Analysis of Metal Deck Shear Diaphragms*. *Proceeding of ASCE. Structure Division* April, 1974.  
 [28] Code for design of cooling tower for industrial recirculating water, GB/T50102-2014.  
 [29] Code for design of steel structure. GB50017-2017.